JYX
JYVÄSKYLÄN YLIOPISTO
UNIVERSITY OF JYVÄSKYLÄ

This is a self-archived version of an original article. This version may differ from the original in pagination and typographic details.

Author(s): Hao, Yuxing; Li, Huanjie; Hu, Guoqiang; Zhao, Wei; Cong, Fengyu

Title: Correcting variance and polarity indeterminacies of extracted components by canonical polyadic decomposition

Year: 2024

Version: Published version

Copyright: © 2024 The Author(s). Published by Informa UK Limited, trading as Taylor & Franci

Rights: CC BY-NC 4.0

Rights url: https://creativecommons.org/licenses/by-nc/4.0/

Please cite the original version:

Hao, Y., Li, H., Hu, G., Zhao, W., & Cong, F. (2024). Correcting variance and polarity indeterminacies of extracted components by canonical polyadic decomposition. Brain-Apparatus Communication, 3(1), Article 2403477.
https://doi.org/10.1080/27706710.2024.2403477

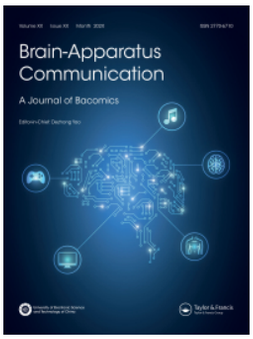

Brain-Apparatus Communication: A Journal of Bacomics

ISSN: (Print) (Online) Journal homepage: www.tandfonline.com/journals/tbac20

Correcting variance and polarity indeterminacies of extracted components by canonical polyadic decomposition

Yuxing Hao, Huanjie Li, Guoqiang Hu, Wei Zhao & Fengyu Cong

To cite this article: Yuxing Hao, Huanjie Li, Guoqiang Hu, Wei Zhao & Fengyu Cong (2024) Correcting variance and polarity indeterminacies of extracted components by canonical polyadic decomposition, Brain-Apparatus Communication: A Journal of Bacomics, 3:1, 2403477, DOI: 10.1080/27706710.2024.2403477

To link to this article: https://doi.org/10.1080/27706710.2024.2403477

© 2024 The Author(s). Published by Informa UK Limited, trading as Taylor & Francis Group.

Published online: 23 Sep 2024.

Submit your article to this journal

View related articles

View Crossmark data

Full Terms & Conditions of access and use can be found at
https://www.tandfonline.com/action/journalInformation?journalCode=tbac20

BRAIN-APPARATUS COMMUNICATION: A JOURNAL OF BACOMICS
2024, VOL. 3, NO. 1, 2403477
https://doi.org/10.1080/27706710.2024.2403477

Taylor & Francis
Taylor & Francis Group

RESEARCH ARTICLE

OPEN ACCESS Check for updates

Correcting variance and polarity indeterminacies of extracted components by canonical polyadic decomposition

Yuxing Hao[a], Huanjie Li[a], Guoqiang Hu[c], Wei Zhao[a] and Fengyu Cong[a,b,d]*

[a]School of Biomedical Engineering, Faculty of Medicine, Dalian University of Technology, Dalian, China; [b]Faculty of Information Technology, University of Jyväskylä, Jyväskylä, Finland; [c]College of Artificial Intelligence, Dalian Maritime University, Dalian, China; [d]Key Laboratory of Social Computing and Cognitive Intelligence (Dalian University of Technology), Ministry of Education, China

ABSTRACT

Background: Back-projection has been used to correct the variance and polarity indeterminacies for the independent component analysis. The variance and polarity of the components are essential features of neuroscience studies.

Objective: This work extends the back-projection theory to canonical polyadic decomposition (CPD) for high-order tensors, aiming to correct the variance and polarity indeterminacies of the components extracted by CPD.

Methods: The tensor is reshaped into a matrix and decomposed using a suitable blind source separation algorithm. Subsequently, the coefficients are projected using back-projection theory, and other factor matrices are computed through a series of singular value decompositions of the back-projection matrix.

Results: By applying this method, the energy and polarity of each component are determined, effectively correcting the variance and polarity indeterminacies in CPD. The proposed method was validated using simulated tensor data and resting-state fMRI data.

Conclusion: Our proposed back-projection method for high-order tensors effectively corrects variance and polarity indeterminacies in CPD, offering a precise solution for calculating the energy and polarity required to extract meaningful features from neuroimaging data.

ARTICLE HISTORY Received 8 August 2023; Accepted 8 September 2024

KEYWORDS Back-projection; blind source separation; canonical polyadic decomposition; tensor

CONTACT Fengyu Cong cong@dlut.edu.cn School of Biomedical Engineering, Faculty of Medicine, Dalian University of Technology, Dalian, China

© 2024 The Author(s). Published by Informa UK Limited, trading as Taylor & Francis Group.
This is an Open Access article distributed under the terms of the Creative Commons Attribution-NonCommercial License (http://creativecommons.org/licenses/by-nc/4.0/), which permits unrestricted non-commercial use, distribution, and reproduction in any medium, provided the original work is properly cited. The terms on which this article has been published allow the posting of the Accepted Manuscript in a repository by the author(s) or with their consent.

1. Introduction

As a crucial method in Brain-Apparatus Communication (BAP) [1], blind source separation (BSS) is extensively utilized to identify and extract latent components of interest from neural signals. And there are some ambiguities, i.e. the variance and polarity indeterminacies for each component and the order indeterminacy of all the components [2]. However, the variance and the polarity of each component can be essential features for some studies, such as analyzing the response to visual stimuli [3] and validating the extracted components from brain signals [4]. The back-projection scheme was proposed to correct the variance indeterminacy [3], and later, complete mathematical details [5–7] were listed when independent component analysis (ICA) was applied. Extensive ICA-based applications also use ICA with back-projection to denoise the pre-processed data [8–11]. The back-projection theory was also introduced to principal component analysis to correct the variance and polarity indeterminacies of principle components [12,13]. However, its applications have mostly been limited to matrices. In the signal processing field, data is often collected in more than two modes, with intrinsic multi-dimensional patterns [14]. Unfolding (matrixing) the high-order tensors into matrices may result in a loss of information. Furthermore, the indeterminacies mentioned above, which exist in high-order tensor decompositions, have been largely overlooked. Correction of the variance indeterminacy of extracted components from tensors by canonical polyadic decomposition (CPD) [15,16] can also be a very significant process to many researches, for example, cognitive neuroscience utilizing functional Magnetic Resonance Imaging (fMRI) [17] and Electroencephalography (EEG) [18], which are two techniques used for studying brain function and the interactions between the brain and external stimuli, that are closely linked to BAC [1, 19].

In this article, we generalize the back-projection theory for the matrix decomposition to high-order tensor decomposition to solve the variance indeterminacy of the extracted components by CPD, one of the most important tensor decomposition models also named parallel factor analysis (PARAFAC) [20]. ICA was ever extended to high-order tensor analysis [17] and a single mode BSS based CPD method was proposed [21]. Unfortunately, they didn't pay more attention to the indeterminacies of the factors from each mode or each component. We adopt this single mode BSS method to achieve the CPD of high-order tensors and solve the indeterminacies by extending the back-projection to high-order tensor decompositions. The high-order tensor is unfolded to a matrix first, then one selected factor matrix is extracted *via* ICA or any other suitable BSS method, and the coefficients of the factor matrix will be projected in

terms of the back-projection theory. Then, the other factor matrices are calculated from the back-projection matrix by a series of singular value decomposition (SVD) [21]. Then, by projecting these factors back to the selected source mode, the back-projection is extended to high-order tensor decompositions. After getting the factor matrix for each mode, the energy of every component can be extracted by utilizing the L2-norm in vector-wise. Through these procedures, we theoretically prove that the variance and polarity indeterminacy of the components extracted by CPD can be corrected by the extended high-order back-projection.

The following notations are adopted. Euler script letters, e.g. $\mathcal{X}$, signifies tensors, and $\mathbf{X}_{(n)}$ signifies the mode-n unfolding (matrixing) of $\mathcal{X}$. Bold capitals (e.g. $\mathbf{U}$) and lowercase letters (e.g. $\mathbf{y}$) signify matrices and vectors, respectively. $\circ$ signifies the outer product of vectors. $\odot$ and $\otimes$ signify the Khatri-Rao product and Kronecker product, respectively.

2. Review of the single mode BSS based CPD

2.1. CPD model

For a given Nth order tensor $\mathcal{X} \in \mathbb{R}^{I_1 \times I_2 \times \cdots \times I_N}$, the CPD model can be characterized as the following equation:

$$\mathcal{X} = \sum_{r=1}^{R} \lambda_r \cdot \mathbf{v}_r^{(1)} \circ \mathbf{v}_{\mathrm{r}}^{(2)} \circ \cdots \circ \mathbf{v}_{\mathrm{r}}^{(\mathrm{N})} + \mathcal{E} = \sum_{\mathrm{r}=1}^{\mathrm{R}} \mathcal{X}_{\mathrm{r}} + \mathcal{E} = \hat{\mathcal{X}} + \mathcal{E}, \tag{1}$$

where $\mathbf{v}_r^{(n)}$ is the rth factor in the mode-n and $\| \mathbf{v}_r^{(n)} \|_2 = 1$ for $r = 1, 2, \ldots, R, n = 1, 2, \ldots, N; \mathcal{X}_r = \lambda_r \cdot \mathbf{v}_r^{(1)} \circ \mathbf{v}_{\mathrm{r}}^{(2)} \circ \cdots \circ \mathbf{v}_{\mathrm{r}}^{(\mathrm{N})} (\mathrm{r} = 1, 2, \ldots, \mathrm{R})$ is the rth component and λ_r is its corresponding scalar; $\hat{\mathcal{X}}$ is the approximate tensor of $\mathcal{X}$ and $\mathcal{E} \in \mathbb{R}^{I_1 \times I_2 \times \cdots \times I_N}$ is the fitting error.

2.2. The single mode BSS method

In this part, we briefly review the single mode BSS based CPD method [21], which will be the fundamental framework for our high-order back-projection theory. For simplicity and without the loss of generality, we take the 3rd-order tensor to introduce our proposed theory. For tensors with more than three modes, only a series of extra SVDs are needed [21]. The back-projection for CPD with an order of any $N > 3$ is listed in Appendix B. The CPD model for 3rd-order tensor is:

$$\mathcal{X} = \sum_{r=1}^{R} \lambda_r \cdot \mathbf{v}_r^{(1)} \circ \mathbf{v}_{\mathrm{r}}^{(2)} \circ \mathbf{v}_{\mathrm{r}}^{(3)} + \mathcal{E}. \tag{2}$$

Let the scalar of each component λ_r be absorbed into the first mode of its corresponding factors. Then we have

$$\mathcal{X} = \sum_{r=1}^{R} \mathbf{u}_r^{(1)} \circ \mathbf{u}_r^{(2)} \circ \mathbf{u}_r^{(3)} + \mathcal{E}, \tag{3}$$

where $\mathbf{u}_r^{(1)} = \lambda_r \mathbf{v}_r^{(1)}, \mathbf{u}_r^{(2)} = \mathbf{v}_r^{(2)}, \mathbf{u}_r^{(3)} = \mathbf{v}_r^{(3)}$.

For Equation (3), the factor matrices of all modes (i.e. $\mathbf{U}^{(n)} = [\mathbf{u}_1^{(n)}, \mathbf{u}_2^{(n)}, \ldots, \mathbf{u}_R^{(n)}], n = 1, 2, 3$) are unknown, where the matrix of every mode can be the source matrix, and matrices of the other modes are regarded as the mixing matrices. Without losing generality, we take the second mode matrix $\mathbf{U}^{(2)}$ as the source matrix here. Taking fMRI data as an example, there are three modes: time, space, and subject, with spatial features assumed to be mutually independent. Before applying a BSS method to the second mode, the tensor data should be structured as a matrix along the second mode:

$$\mathbf{X}_{(2)} \triangleq \left(\mathbf{U}^{(3)} \odot \mathbf{U}^{(1)}\right) \cdot \mathbf{U}^{(2)^T} = \mathbf{A}^{(2)} \cdot \mathbf{U}^{(2)^T}, \tag{4}$$

where $\mathbf{A}^{(2)} = \mathbf{U}^{(3)} \odot \mathbf{U}^{(1)} = [\mathbf{a}_1^{(2)}, \mathbf{a}_2^{(2)}, \ldots, \mathbf{a}_R^{(2)}] \in \mathbb{R}^{I_1 I_3 \times R}$ and $\mathbf{a}_r^{(2)} = \mathbf{u}_r^{(3)} \otimes \mathbf{u}_r^{(1)}$. Then (4) becomes a classical BSS problem. The CPD model for 3rd-order fMRI data and its matrixing is shown in Figure 1. Actually, the matrixed fMRI data is the concatenated data from multiple subjects along the subject dimension [22].

Then, the source matrix $\mathbf{U}^{(2)^T}$ can be estimated as:

$$\mathbf{Y}^{(2)} = \mathbf{W}\mathbf{X}_{(2)} = [\mathbf{y}_1^{(2)}, \mathbf{y}_2^{(2)}, \ldots, \mathbf{y}_R^{(2)}]^T \in \mathbb{R}^{R \times I_2}, \tag{5}$$

where $\mathbf{W} \in \mathbb{R}^{R \times I_1 I_3}$ is the unmixing matrix generated by a BSS algorithm (usually $I_1 I_3$ is far larger than R). From (4) and (5) we have

$$\mathbf{Y}^{(2)} = \mathbf{W}\mathbf{A}^{(2)} \cdot \mathbf{U}^{(2)^T} = \mathbf{C}\mathbf{U}^{(2)^T}, \tag{6}$$

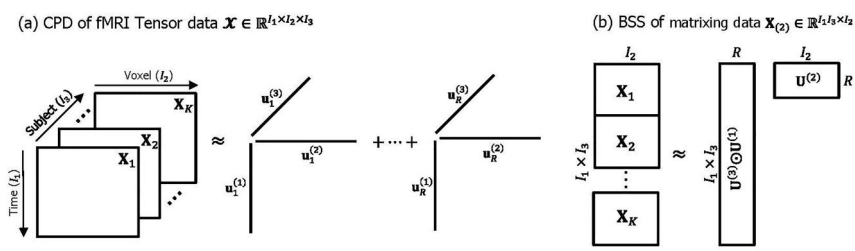

Figure 1. Illustration of CPD for multi-subject fMRI data and BSS for its matrixing data.

where $\mathbf{C} \in \mathbb{R}^{R\times R}$ is the global matrix, of which only one nonzero element existing in each row and each column under a suitable BSS method with the theoretically global optimization [5,6]. Then we have

$$\mathbf{y}_p^{(2)} = c_{p,q}\mathbf{u}_q^{(2)}, \tag{7}$$

where $c_{p,q}$ is the only one nonzero element in pth row and qth column of the global matrix $\mathbf{C}$. Let $\mathbf{B} = [\mathbf{b}_1, \mathbf{b}_2, \ldots, \mathbf{b}_R] \in \mathbb{R}^{I_1 I_3 \times R}$ denotes the pseudoinverse matrix of $\mathbf{W}$. Then we have

$$\mathbf{b}_p = \mathbf{a}_q^{(2)} c_{p,q}^{-1}, \tag{8}$$

which means $\mathbf{b}_p$ is just a scaling of $\mathbf{a}_q^{(2)}$. Construct a matrix $\mathbf{B}_p$ by reshaping $\mathbf{b}_p$ to a matrix such that

$$\mathbf{B}_p = c_{p,q}^{-1}\mathbf{u}_q^{(3)} \circ \mathbf{u}_{\mathrm{q}}^{(1)}, \tag{9}$$

where $\mathbf{B}_p$ is a matrix of rank-1. As the SVD of a rank-1 matrix is essentially unique, the left singular vector is the scaling of $\mathbf{u}_q^{(3)}$ and the right singular vector is the scaling of $\mathbf{u}_q^{(1)}$ (more details are listed in Appendix A). Recovering the factors form the other modes form (8) and (9) could also be regarded as the inverse of Khatri-Rao Product. In sum, we can have a good estimation of all the factor matrices. However, the indeterminacies of scaling and permutation of their columns are unavoidable. Thus the variance and polarity indeterminacies still existing for this single mode BSS based CPD method [21].

3. Back-projection for correcting the indeterminacies

In this part, we introduce our novel method for solving the variance indeterminacy of every single extracted component by CPD in the case of a high-order tensor by extending the back-projection in the matrix decomposition [5–7] to high-order tensor decomposition.

First, after projecting the pth column of the back-projection matrix $\mathbf{B}$ to the pth estimated source, we have

$$\mathbf{b}_p \circ \mathbf{y}_{\mathrm{p}}^{(2)} = \mathbf{a}_{\mathrm{q}}^{(2)} \mathbf{c}_{\mathrm{p,q}}^{-1} \circ \mathbf{c}_{\mathrm{p,q}} \mathbf{u}_{\mathrm{q}}^{(2)} = \mathbf{a}_{\mathrm{q}}^{(2)} \circ \mathbf{u}_{\mathrm{q}}^{(2)}, \tag{10}$$

the back-projection equation of the BSS with two modes of a matrix. As $\mathbf{y}_p^{(2)}$ is the estimation of one source, its corresponding vector contains the information of all the other modes. Then by matrixing $\mathbf{b}_p$ and $\mathbf{a}_q^{(2)}$, we have $\mathbf{B}_p$ and $\mathbf{u}_q^{(3)} \circ \mathbf{u}_{\mathrm{q}}^{(1)}$. These two matrices are of rank-1 and just with scaling ambiguity. From Equation (9), we have the rank-1 decomposition of $\mathbf{B}_p$:

$$\mathbf{B}_p = \mathbf{y}_p^{(3)} \circ \mathbf{y}_{\mathrm{p}}^{(1)} = \mathbf{c}_{\mathrm{p,q}}^{-1} \mathbf{u}_{\mathrm{q}}^{(3)} \circ \mathbf{u}_{\mathrm{q}}^{(1)}. \tag{11}$$

Then from Equations (7) and (11) we have

$$\mathbf{y}_p^{(3)} \circ \mathbf{y}_p^{(1)} \circ \mathbf{y}_p^{(2)} = \mathbf{u}_q^{(3)} \circ \mathbf{u}_q^{(1)} \circ \mathbf{u}_q^{(2)}, \tag{12}$$

which $\mathbf{y}_p^{(i)}$ and $\mathbf{u}_q^{(i)}$ are colinear $(i = 1, 2, 3)$, and the order of the modes could be arranged in sequence:

$$\mathbf{y}_p^{(1)} \circ \mathbf{y}_p^{(2)} \circ \mathbf{y}_p^{(3)} = \mathbf{u}_q^{(1)} \circ \mathbf{u}_q^{(2)} \circ \mathbf{u}_q^{(3)}. \tag{13}$$

Then we have

$$\| \mathbf{y}_p^{(1)} \|_2 \| \mathbf{y}_p^{(2)} \|_2 \| \mathbf{y}_p^{(3)} \|_2 = \| \mathbf{u}_q^{(1)} \|_2 \| \mathbf{u}_q^{(2)} \|_2 \| \mathbf{u}_q^{(3)} \|_2. \tag{14}$$

Equations (13) and (14) are the back-projection equations of high-order tensor decompositions. According to the high-order back-projection theory for CPD, the energies (variances) of the rank-1 tensor components are determined (Equation (14)). The energy definition of the pth component is as follows:

$$\lambda_p = \| \mathbf{y}_p^{(1)} \|_2 \| \mathbf{y}_p^{(2)} \|_2 \| \mathbf{y}_p^{(3)} \|_2. \tag{15}$$

Then the energy of every component can be determined and equals to its corresponding inherent one theoretically. And the polarity indeterminacy also emerges in Equation (12), in fact, if the first mode was selected to identify the polarity of features, then the source of pth component in the first mode and its corresponding qth estimation in global optimization could be mapped and projected as

$$y_{i_2 p}^{(2)} \cdot y_{i_3 p}^{(3)} \cdot \mathbf{y}_p^{(1)} = u_{i_2 q}^{(2)} \cdot u_{i_3 q}^{(3)} \cdot \mathbf{u}_q^{(1)}, \tag{16}$$

for any $i_2 \in \{1, 2, \ldots, I_2\}, i_3 \in \{1, 2, \ldots, I_3\}$.

4. Datasets

4.1. Simulation

To verify the correction of variance indeterminacy by our tensor back-projection theory, we formed a 3rd-order fMRI-like tensor data and its decomposition results under global optimization, i.e. every decomposition result is obtained by a proper BSS algorithm, and the columns in any mode's factor matrix only have scaling and permutation ambiguity. The fMRI-like data was formed by selecting ten spatially independent components (networks) (67541 grey matte voxels for each component) [23] and ten serials (1000 points per serial) as the corresponding time courses from the ICALAB [24] (Figure 2). The spatial networks were found to have potential functional relevance, consisting of regions involved in motor function, auditory processing, memory, and the default-mode

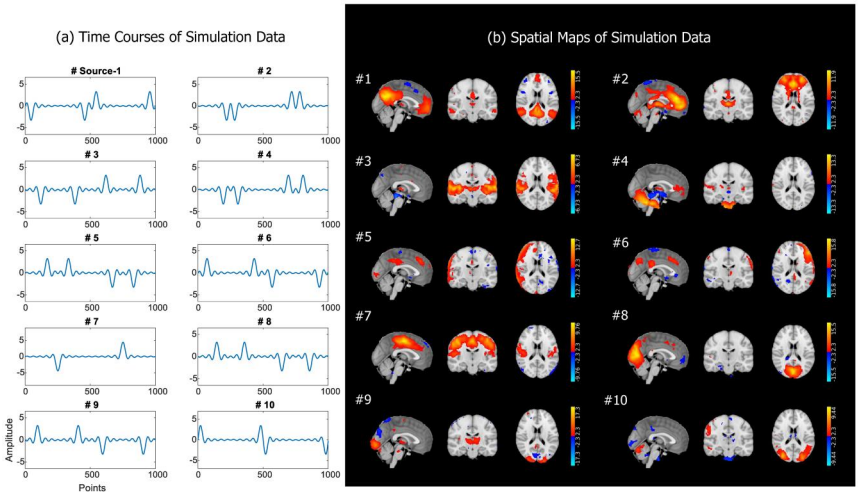

Figure 2. Simulated time courses and spatial maps for fMRI-like data.

network [23]. Moreover, the third mode was assumed as the subject mode, with entries generated randomly in a restricted range with positive numbers (the series are relatively uncorrelated from each other), i.e. the CPD model allows each subject to have its specific parameters for their common components (spatial maps and time courses) [17, 22]. Then, by combining these three modes with an identity core tensor, the third-order tensor fMRI-like data was obtained. Some basic tensor operations were adopted from the Tensrorlab [25].

Global optimization is an ideal case for theoretical analysis, so obtaining global optimization is not achievable when running ICA algorithms. We also decomposed the simulated fMRI-like tensor data to obtain locally optimized decomposition results using the single-mode BSS method [21]. As one of the classical BSS methods, ICA is a data-driven method widely applied for medical signal processing, especially for analyzing fMRI datasets. The tensor fMRI-like data was unfolded along the spatial mode into a matrix first, and then the InfomaxICA [26,29] method was utilized to find the estimation of the spatial sources. After obtaining the back-projection matrix, the sources of the other two modes were estimated by Equations (10) and (11).

4.2. Resting-state fMRI data

We selected resting-state fMRI data of 4 participants scanned at five different centers in the DecNef Project Brain Data Repository (https://bicr-resource.atr.jp/srpbsts/) to form a 3rd-order tensor of time * space *

subjects for testing the back-projection theory. The data were collected during rest with the following scan parameters: TR: 2.5 s, TE: 30 ms, Flip angle: 80 deg, Phase encoding: PA, Matrix: 64×64, FOV: 212 mm, In-plane resolution: 3.3×3.3 mm [27]. Due to varying scan counts per participant (ranging from 234 to 230), data exceeding 230 scans were trimmed for consistency across all datasets. Data preprocessing was completed with the DPABI [28] for slice timing correction, realignment for motion correction, and spatial normalization to MNI standard space. Temporal band pass filtering 0.01–0.1 Hz was applied to the data.

We applied the single-mode BSS method for the real fMRI data, and InfomaxICA was selected to extract the independent spatial maps from the matrixed data. After obtaining the spatial maps and their coefficients (the back-projection matrix), the sources of the temporal and subject modes were estimated by Equations (10) and (11).

5. Results

5.1. Results of simulated data

Figure 3 shows the global matrix under global and local optimization, respectively. For the global optimization case, there is precisely one nonzero entry in each row and each column of the global matrix. For the local optimization case, the global matrix has only one element with a comparatively large absolute value in each row and column, and this covers the locally optimized CP decomposition [6].

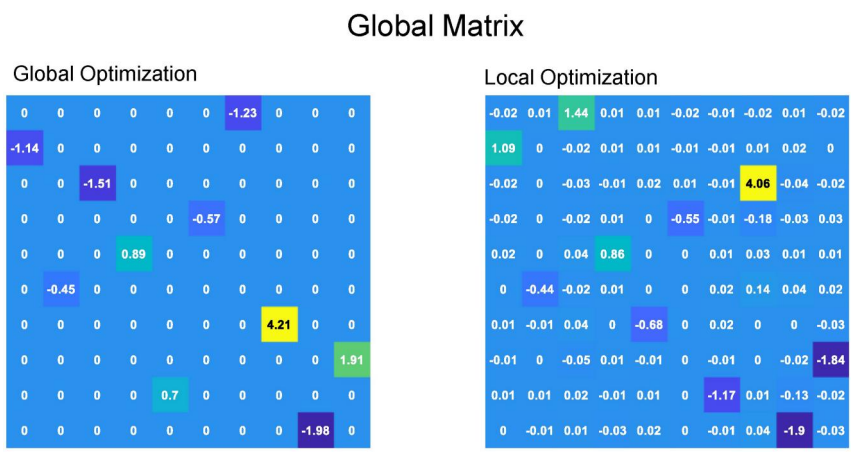

Figure 3. Global matrix under global optimization and local optimization. Under global optimization, there is only one nonzero element in each row and column of the global matrix; for local optimization, there is only one element with a comparatively large absolute value in each row and column.

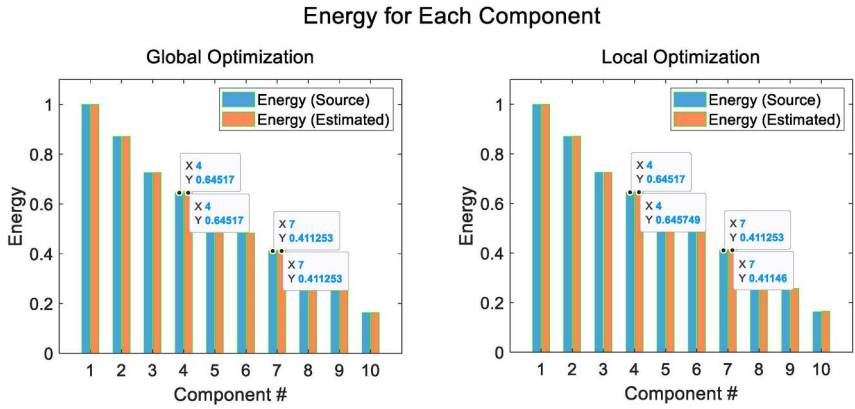

Figure 4. The energy of each component under (a) global optimization and (b) local optimization.

The energies for all the estimated components were computed by Equation (15) to validate the correction of the variance indeterminacy. After unifying the order of the sources and the estimations in descending way, the energy for every source component and its estimation were completely identical under global optimization. As the global matrix simulated under local optimization has only one element with a comparatively large absolute value in each row and each column, the energy for every source component and its estimation were almost identical (Figure 4).

Besides, the correlation between the sources and estimations was calculated along each mode to check the indeterminacy of polarity. We also calculated the Hadamard product that combines all the correlation matrices for all modes to form the component correlation coefficients, and the polarity indeterminacy automatically emerged as we analyzed from Equations (12) and (16) (Figure 5). Then, the first mode of the simulated fMRI-like data was used to assess the correction of polarity indeterminacy. The projected courses are shown in Figure 6 and the index of the other modes, i.e. i_2 and i_3, are randomly selected. Under global optimization, the projections in the first mode were completely identical between the sources and their global estimations. Though the polarity of the projections was corrected under local optimization, the amplitudes may not be completely identical between some of the local estimations and sources.

5.2. Results of resting-state fMRI data validation

For the real third-order tensor data, 15 components were selected, and single-model blind source separation was performed 30 times. The results

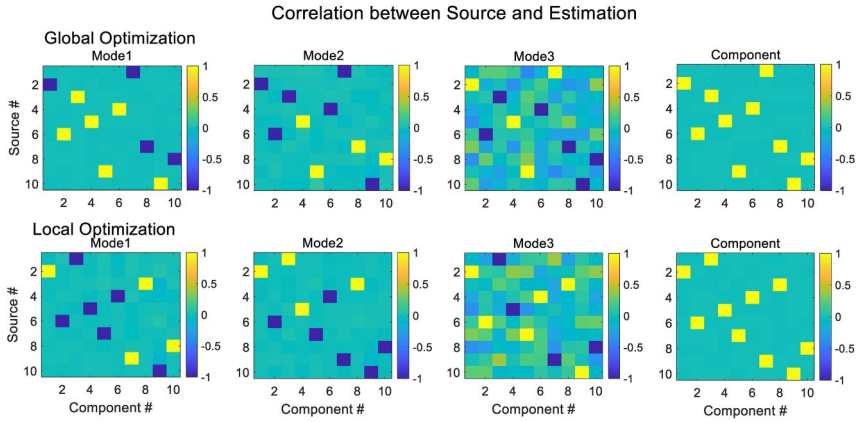

Figure 5. The correlation matrix of the three modes and the whole components under global and local optimization, respectively.

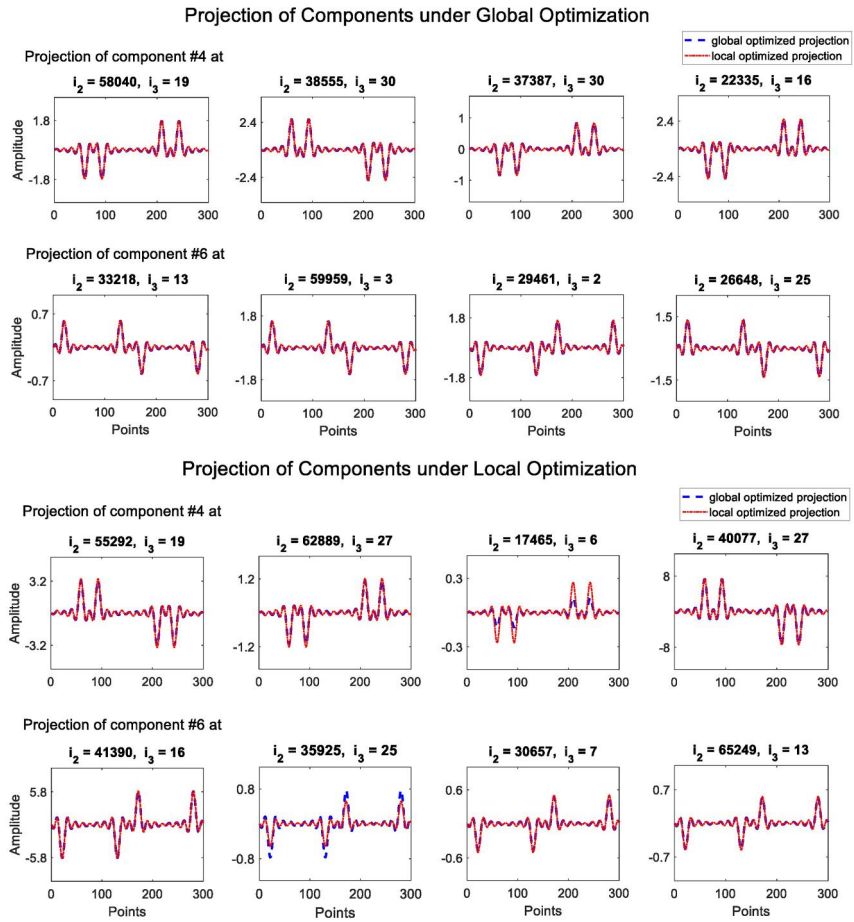

Figure 6. Projection of two components to the first mode. (source data and the estimation data).

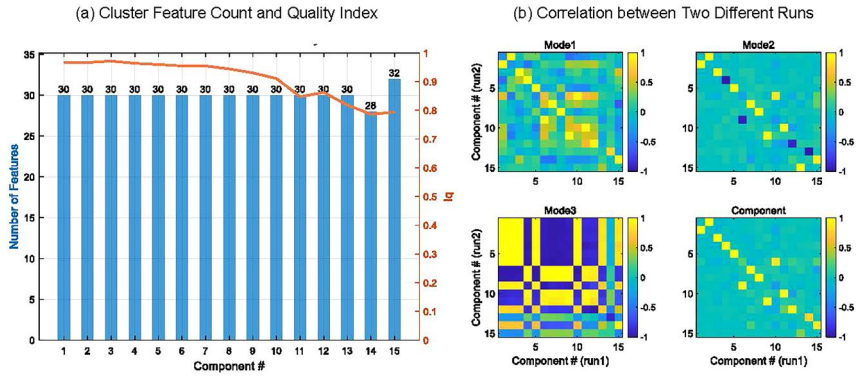

Figure 7. The clustering results of multiple runs and the correlation between two different runs. (a) Cluster feature count and quality index. (b) Correlations between two different runs.

of clustering estimated independent components using agglomerative hierarchical clustering are shown in Figure 7(a), where I_q represents the difference between the within-class average similarity (absolute value of Pearson correlation coefficient) and the between-class average similarity. For the first few clusters, the I_q values are relatively close to 1, whereas for the later clusters, the I_q values are relatively lower, and there is a slight deviation in the number of features in the last two clusters. Figure 7(b) shows the correlation matrix for each mode and the whole component. For each mode, the Pearson correlation coefficients were calculated for all features in two different runs to form the correlation matrix. For the whole component, the correlation was calculated for the tensor components (reshaped as a long vector) in different runs, and the polarity indeterminacy was removed. Due to the statistical independence constraint applied to the matrix factorization of the second mode, the matrix factors of the other two modes exhibited correlated components. However, this correlation did not affect the elimination of polarity indeterminacy.

Figure 8(a) compares the energies of the same component under different runs, and the corresponding values for the same component were roughly identical. The variance and polarity of the two loadings were different in different runs (Figure 8(b)). Then, the subject mode was used to assess the correction of polarity indeterminacy. Under two randomly selected indexes of the other two modes, the polarity indeterminacy of the loadings was corrected, while the variance indeterminacy was not corrected well in real data analysis (Figure 8(c)).

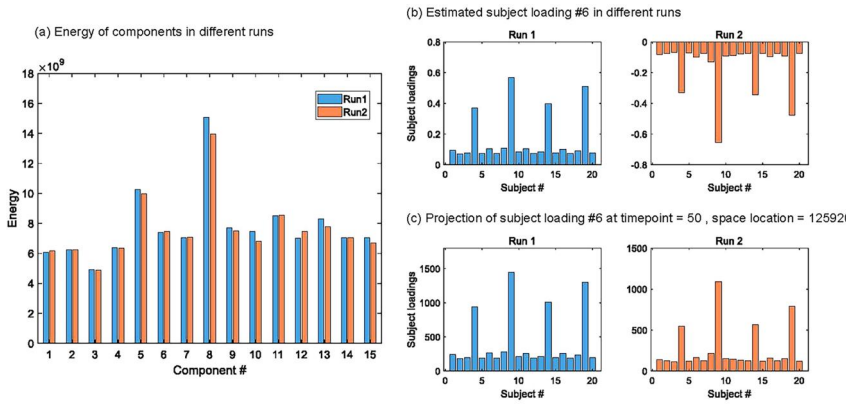

Figure 8. (a) The energy of each component in two different runs. (b) The estimated subject loading #6 in two different runs. (c) The projected loadings at specific timepoint and space location.

6. Conclusion

In this article, encouraged by the back-projection of ICA to solve the variance and polarity indeterminacies, we extended it to the single mode BSS based CPD for high-order tensors. We formed the one-to-one correspondence between the inherent components and the estimated components, evaluated the estimated energy for every single component, and theoretically solved the indeterminacy problem of variance and polarity for every component. From the simulation data, we validated the theory successfully under global optimization. We also tested the theory in local optimization for simulated data and real fMRI data analysis, the variance and polarity indeterminacies were corrected effectively. It is promising that our proposed high-order back-projection theory for CPD can be applied to some real-world neuroscience data decomposition.

Disclosure statement

We declare that we have no known competing financial interests or personal relationships that could have appeared to influence the work presented in this manuscript.

Funding

This work was supported by the National Natural Science Foundation of China [grant numbers 91748105 & 81471742], the Science and Technology Planning Project of Liaoning Provincial [grant numbers 2022JH2/10700002 and 2021JH1/10400049], and the scholarship from China Scholarship Council (No. 202306060039).

Data availability statement

The data used for simulation are from http://www.bsp.brain.riken.jp/ICALAB and https://doi.org/10.1073/pnas.0601417103. The resting-state fMRI data used in this study are publicly available from the DecNef Project Brain Data Repository website (https://bicr-resource.atr.jp/srpbsts/).

References

1 Yao D, Zhang Y, Liu T, et al. Bacomics: a comprehensive cross area originating in the studies of various brain–apparatus conversations. Cogn Neurodyn. 2020;14(4):425–442. doi: 10.1007/s11571-020-09577-7.

2 Hyvärinen A, Oja E. Independent component analysis: algorithms and applications. Neural Netw. 2000;13(4–5):411–430. doi: 10.1016/s0893-6080(00) 00026-5.

3 Makeig S, Westerfield M, Jung T-P, et al. Functionally independent components of the late positive event-related potential during visual spatial attention. J Neurosci. 1999;19(7):2665–2680. doi: 10.1523/JNEUROSCI.19-07-02665.1999.

4 Calhoun VD, Adali T, Pearlson GD, et al. A method for making group inferences from functional MRI data using independent component analysis. Hum Brain Mapp. 2001;14(3):140–151. doi: 10.1002/hbm.1048.

5 Cong F, Kalyakin I, Chang Z, et al. Analysis on subtracting projection of extracted independent components from EEG recordings. Biomed Tech (Berl). 2011;56(4):223–234. doi: 10.1515/BMT.2011.102.

6 Cong F, Kalyakin I, Ristaniemi T. Can back-projection fully resolve polarity indeterminacy of independent component analysis in study of event-related potential? Biomed Signal Process Control. 2011;6(4):422–426. doi: 10.1016/j.bspc.2010.05.006.

7 Cong F, He Z, Hämäläinen J, et al. Validating rationale of group-level component analysis based on estimating number of sources in EEG through model order selection. J Neurosci Methods. 2013;212(1):165–172. doi: 10.1016/j.jneumeth.2012.09.029.

8 Chen J, Liu J, Calhoun VD, et al. Exploration of scanning effects in multi-site structural MRI studies. J Neurosci Methods. 2014;230:37–50. doi: 10.1016/j.jneumeth.2014.04.023.

9 Delorme A, Makeig S. EEGLAB: an open source toolbox for analysis of single-trial EEG dynamics including independent component analysis. J Neurosci Methods. 2004;134(1):9–21. doi: 10.1016/j.jneumeth.2003.10.009.

10 Hao Y, Xu H, Xia M, et al. Removal of site effects and enhancement of signal using dual projection independent component analysis for pooling multi-site MRI data. Eur J Neurosci. 2023;58(6):3466–3487. doi: 10.1101/2023.04.26.538366.

11 Xu H, Hao Y, Zhang Y, et al. Harmonization of multi-site functional MRI data with dual-projection based ICA model. Front Neurosci. 2023;17:1225606. doi: 10.3389/fnins.2023.1225606.

12 Zhang G, Li X, Lu Y, et al. Single-trial-based temporal principal component analysis on extracting event-related potentials of interest for an individual subject. J Neurosci Methods. 2023;385:109768. doi: 10.1016/j.jneumeth.2022.109768.

13 Zhang G, Li X, Cong F. Objective extraction of evoked event-related oscillation from time-frequency representation of event-related potentials. Neural Plast. 2020;2020(1):8841354. doi: 10.1155/2020/8841354.
14 Cichocki A, Mandic D, De Lathauwer L, et al. Tensor decompositions for signal processing applications: from two-way to multiway component analysis. IEEE Signal Process Mag. 2015;32(2):145–163. doi: 10.1109/MSP.2013.2297439.
15 Carroll JD, Chang JJ. Analysis of individual differences in multidimensional scaling via an n-way generalization of "Eckart-Young" decomposition. Psychometrika. 1970;35(3):283–319. doi: 10.1007/BF02310791.
16 Hitchcock FL. Multiple invariants and generalized rank of a P-way matrix or tensor. J Math Phys. 1928;7(1–4):39–79. doi: 10.1002/sapm19287139.
17 Beckmann CF, Smith SM. Tensorial extensions of independent component analysis for multisubject FMRI analysis. Neuroimage. 2005;25(1):294–311. doi: 10.1016/j.neuroimage.2004.10.043.
18 Cong F, Lin QH, Kuang LD, et al. Tensor decomposition of EEG signals: a brief review. J Neurosci Meth. 2015;248:59–69. doi: 10.1016/j.jneumeth.2015.03.018.
19 Tang Y, Duan M, Tan S, et al. The response of hippocampal functional connectivity to sustained pain in a pain-sensitive population. Brain-Apparatus Commun A J Bacomics. 2023;2:2185105.
20 Harshman R A. Foundations of the PARAFAC procedure: models and conditions for an "explanatory" multi-modal factor analysis. UCLA Work Pap Phonetics. 1970:16(1):1–84. http://www.psychology.uwo.ca/faculty/harshman/wpppfac0.pdf.
21 Zhou G, Cichocki A. Canonical polyadic decomposition based on a single mode blind source separation. IEEE Signal Process Lett. 2012;19(8):523–526. doi: 10.1109/LSP.2012.2205237.
22 Calhoun VD, Liu J, Adali T. A review of group ICA for fMRI data and ICA for joint inference of imaging, genetic, and ERP data. Neuroimage. 2009;45(1 Suppl):S163–S172. doi: 10.1016/j.neuroimage.2008.10.057.
23 Damoiseaux JS, Rombouts SARB, Barkhof F, et al. Consistent resting-state networks across healthy subjects. Proc Natl Acad Sci USA. 2006;103(37):13848–13853. doi: 10.1073/pnas.0601417103.
24 Cichocki A. ICALAB toolboxes; 2004. http://www.bsp.brain.riken.jp/ICALAB.
25 Vervliet N, Debals O, Sorber L, et al. Tensorlab user guide release 3.0; 2016. http://www.tensorlab.net. https://www.tensorlab.net/doc/.
26 Himberg J, Hyvärinen A, Esposito F. Validating the independent components of neuroimaging time series via clustering and visualization. Neuroimage. 2004;22(3):1214–1222. doi: 10.1016/j.neuroimage.2004.03.027.
27 Tanaka SC, Yamashita A, Yahata N, et al. A multi-site, multi-disorder resting-state magnetic resonance image database. Sci Data. 2021;8(1):227. doi: 10.1038/s41597-021-01004-8.
28 Yan C, Wang X, Zuo X, et al. DPABI: data processing & analysis for (resting-state) brain imaging. Neuroinformatics. 2016;14(3):339–351. doi: 10.1007/s12021-016-9299-4.
29 Bell AJ, Sejnowski TJ. An information-maximization approach to blind separation and blind deconvolution. Neural Comput. 1995;7(6):1129–1159. doi: 10.1162/neco.1995.7.6.1129.

Appendix A

A. 1. Khatri-Rao product

The Kronecker product of two matrices $\mathbf{A} \in R^{I\times J}$ and $\mathbf{B} \in \boldsymbol{R}^{K\times L}$ is

$$\mathbf{A} \otimes \mathbf{B} = \begin{bmatrix} a_{11}\mathrm{B} & a_{12}\mathrm{B} & \dots & a_{1J}\mathrm{B} \\ a_{21}\mathrm{B} & a_{22}\mathrm{B} & \dots & a_{2J}\mathrm{B} \\ \vdots & \vdots & \ddots & \vdots \\ a_{I1}\mathrm{B} & a_{I2}\mathrm{B} & \dots & a_{IJ}\mathrm{B} \end{bmatrix} \in R^{IK} \times JL. \tag{A.1}$$

And the Khatri-Rao product of two matrices $\mathbf{A} \in R^{I\times J}$ and $\mathbf{B} \in \boldsymbol{R}^{K\times J}$ (the number of columns of these two matrices should be identical) is a matrix defined as:

$$\mathbf{A}\odot\mathbf{B} = [\mathbf{a}_1 \otimes \mathbf{b}_1, \mathbf{a}_2 \otimes \mathbf{b}_2, \ \dots, \mathbf{a}_J \otimes \mathbf{b}_J] \in \mathrm{R}^{\mathrm{IK}} \times \boldsymbol{J}, \tag{A.2}$$

which can be considered as the column-wise of Kronecker product.

A.2. The uniqueness of SVD for rank-1 matrix

Given a $m \times n$ $(m \geq n)$ real matrix $\mathbf{A}$, its singular value decomposition is defined as the following equation

$$\mathbf{A} = \mathbf{U}\boldsymbol{\Sigma}\mathbf{V}^T, \tag{A.3}$$

where $\mathbf{U} = [\mathbf{u}_1, \mathbf{u}_2, \dots, \mathbf{u}_m]$ is a $m \times m$ orthogonal matrix, $\mathbf{V} = [\mathbf{v}_1, \mathbf{v}_2, \dots, \mathbf{v}_n]$ is a $n \times n$ orthogonal matrix; The diagonal elements, $\sigma_1, \sigma_2, \dots, \sigma_n$, of $\boldsymbol{\Sigma}$ are the singular values of $\mathbf{A}$, and $\sigma_1 \geq \sigma_2 \geq \dots \geq \sigma_n \geq 0$.

In matrix summation form, Equation (A.3) can be transformed into:

$$\mathbf{A} = \sum_{k=1}^{n} \sigma_k \cdot \mathbf{u}_k \cdot \mathbf{v}_k{}^T. \tag{A.4}$$

If $\sigma_1 \geq \sigma_2 \geq \dots \geq \sigma_m > \sigma_{m+1} = \dots = \sigma_n = 0, \mathrm{m} < \mathrm{n}$, then we have the truncated SVD of $\mathbf{A}$:

$$\mathbf{A} = \sum_{k=1}^{m} \sigma_k \cdot \mathbf{u}_k \cdot \mathbf{v}_k{}^T. \tag{A.5}$$

The truncated SVD of a matrix is essentially unique. Especially, if $\mathbf{A}$ is a matrix of rank-1, then $\frac{1}{\sigma_1}\mathbf{A} = \mathbf{u}_1 \cdot \mathbf{v}_1{}^T$ and $\| \mathbf{u}_1\|_2 = 1, \ \| \mathbf{v}_1\|_2 = 1, \ \| \mathbf{u}_1 \cdot \mathbf{v}_1{}^T\|_2 = 1$.

If there are also two different column-wise vectors, $\mathbf{a}, \mathbf{b}$ satisfy $\| \mathbf{a}\cdot\mathbf{b}_1{}^T \|_2 = 1$ and $\frac{1}{\sigma_k}\mathbf{A} = \mathbf{a} \cdot \mathbf{b}^T$, then we have

$$\mathbf{a} = \frac{1}{c}\mathbf{u}_1, \mathbf{b} = c\mathbf{v}_1 \tag{A.6}$$

where c is a non-zero scalar.

Proof:

$$\frac{1}{\sigma_k}\mathbf{A} \cdot \mathbf{v}_1 = \mathbf{u}_1 \cdot \mathbf{v}_1{}^T \cdot \mathbf{v}_1 = \mathbf{u}_1 \tag{A.7}$$

$$\frac{1}{\sigma_k}\mathbf{A}\cdot\mathbf{v}_1=\mathbf{a}\cdot\mathbf{b}^T\cdot\mathbf{v}_1=\mathbf{a}\cdot\left(\mathbf{b}^T\cdot\mathbf{v}_1\right)=c\mathbf{a}, \tag{A.8}$$

where $c=\mathbf{b}^T\cdot\mathbf{v}_1$. Then from Equations (A.7) and (A.8) we have $\mathbf{a}=\frac{1}{c}\mathbf{u}_1$.

Then we have

$$\mathbf{u}_1{}^T\cdot\mathbf{a}\cdot\mathbf{b}^T=\mathbf{u}_1{}^T\cdot\mathbf{a}\cdot\mathbf{b}^T=\frac{1}{c}\mathbf{b}^T, \tag{A.9}$$

and

$$\mathbf{u}_1{}^T\cdot\mathbf{a}\cdot\mathbf{b}^T=\mathbf{u}_1{}^T\cdot\mathbf{u}_1\cdot\mathbf{v}_1{}^T=\mathbf{v}_1{}^T. \tag{A.10}$$

Then, from Equations (A.9) and (A.10), we have $\mathbf{b}=c\mathbf{v}_1$.

Appendix B. Back-projection for CPD with mode N > 3

B.1. Review of the single mode BSS based CPD for N-way tensor

The CPD model for Nth-order tensor $\mathcal{X}\in\mathbb{R}^{I_1\times I_2\times\cdots\times I_N}$ is

$$\mathcal{X}=\sum_{r=1}^{R}\lambda_r\cdot\mathbf{v}_r^{(1)}\circ\mathbf{v}_{\mathrm{r}}^{(2)}\circ\ldots\circ\mathbf{v}_{\mathrm{r}}^{(\mathrm{N})}+\mathcal{E}. \tag{B.1}$$

Let the scalar of each component λ_r be absorbed into the nth mode of its corresponding factors. Then we have

$$\mathcal{X}=\sum_{r=1}^{R}\mathbf{u}_r^{(1)}\circ\mathbf{u}_{\mathrm{r}}^{(2)}\circ\ldots\circ\mathbf{u}_{\mathrm{r}}^{(\mathrm{N})}+\mathcal{E}, \tag{B.2}$$

where $\mathbf{u}_r^{(n)}=\lambda_r\mathbf{v}_r^{(n)}$ and $\mathbf{u}_r^{(n)}=\mathbf{v}_r^{(n)}$ for $n=1,2,\ldots,n-1,n+1,\ldots,N$. And the mode-n matrixing of $\mathcal{X}$ is

$$\mathbf{X}_{(n)}\triangleq\mathbf{A}^{(n)}\cdot\mathbf{U}^{(n)^T}\in\mathbb{R}^{(I_N\times\cdots\times I_{n+1}\times I_{n-1}\times\cdots\times I_1)\times I_n}, \tag{B.3}$$

where $\mathbf{A}^{(n)}=\odot_{k\neq n}\mathbf{U}^{(n)}$, and $\mathbf{U}^{(n)}$ is the source matrix. Then we can use a BSS method to calculate an unmixing matrix $\mathbf{W}$ to estimate the source from Equation (B.3) such that

$$\mathbf{Y}^{(n)}=\mathbf{W}\mathbf{X}_{(n)}=[\mathbf{y}_1^{(n)},\mathbf{y}_2^{(n)},\ldots,\mathbf{y}_R^{(n)}]^T\in\mathbb{R}^{R\times I_n}. \tag{B.4}$$

Then we have

$$\mathbf{Y}^{(n)}=\mathbf{W}\mathbf{A}^{(n)}\cdot\mathbf{U}^{(n)^T}=\mathbf{C}\mathbf{U}^{(n)^T}, \tag{B.5}$$

where $\mathbf{C}\in\mathbb{R}^{R\times R}$ is the global matrix, of which only one nonzero element existing in each row and each column under a suitable BSS method with the theoretically global optimization. Then we have

$$\mathbf{y}_p^{(n)}=c_{p,q}\mathbf{u}_q^{(n)}, \tag{B.6}$$

where $c_{p,q}$ is the only one nonzero element in pth row and qth column of the global matrix $\mathbf{C}$, indicating that the uniqueness for the features along each mode of the tensor is still up to a scalar indeterminacy even the estimation is under the global optimization.

Let $\mathbf{B} = [\mathbf{b}_1, \mathbf{b}_2, \ldots, \mathbf{b}_R] \in \mathbb{R}^{(I_N \times \cdots \times I_{n+1} \times I_{n-1} \times \cdots \times I_1) \times R}$ denotes the pseudoinverse matrix of $\mathbf{W}$. Then we have

$$\mathbf{b}_p = \mathbf{a}_q^{(n)} c_{p,q}^{-1}, \tag{B.7}$$

thus $\mathbf{b}_p$ is just a scaling of $\mathbf{a}_q^{(n)}$. And from Equation (B.3) the qth column of A could de denoted as

$$\mathbf{a}_q^{(n)} = \otimes_{k \neq n} \mathbf{u}_q^{(n)}. \tag{B.8}$$

Then $\mathbf{u}_q^{(n)}$ could be calculated from a series of SVD of rank-1 matrices.

B.2. Back-projection for correcting the indeterminacies

Then, we extend the back-projection theory to Nth-order CPD.

Firstly, projecting the pth column of the back-projection matrix $\mathbf{B}$ to the pth estimated source, we have

$$\mathbf{b}_p \circ \mathbf{y}_{\mathrm{p}}^{(\mathrm{n})} = \mathbf{a}_{\mathrm{q}}^{(\mathrm{n})} \mathbf{c}_{\mathrm{p,q}}^{-1} \circ \mathbf{c}_{\mathrm{p,q}} \mathbf{u}_{\mathrm{q}}^{(\mathrm{n})} = \mathbf{a}_{\mathrm{q}}^{(\mathrm{n})} \circ \mathbf{u}_{\mathrm{q}}^{(\mathrm{n})}, \tag{B.9}$$

the back-projection equation of the BSS with two modes of a matrix. As $\mathbf{y}_p^{(n)}$ is the estimation of one source, its corresponding vector $\mathbf{b}_p$ contains the information of all the other $N-1$ modes. Reshaping $\mathbf{b}_p$ to a matrix of size $(I_N, I_{N-1} \times \cdots \times I_{n+1} \times I_{n-1} \times \cdots \times I_1)$, and from Equations (B.7) and (B.8) we have

$$\mathbf{B}_p^{N-2} = c_{p,q}^{-1} \mathbf{u}_q^{(N)} \circ \left(\otimes_{k \neq n,\, \mathrm{N}} \mathbf{u}_{\mathrm{q}}^{(\mathrm{n})} \right), \tag{B.10}$$

where $\mathbf{B}_p^{N-2} \in \mathbb{R}^{I_N \times (I_{N-1} \times \cdots I_{n+1} \times I_{n-1} \times \cdots \times I_1)}$ is the matrix of rank-1 reshaped from $\mathbf{b}_p$, and $N-2$ here just symbols the column of $\mathbf{B}_p^{N-2}$ containing the information from $N-2$ mode of the tensor. As the rank-1 SVD is essentially unique for a rank-1 matrix, we can estimate $\mathbf{u}_q^{(N)}$ up to a scalar indeterminacy by the left singular vector $\mathbf{y}_p^{(N)}$:

$$\mathbf{B}_p^{N-2} = \mathbf{y}_p^{(N)} \circ \mathbf{b}_{\mathrm{p}}^{(\mathrm{N}-2)} = \mathbf{c}_{\mathrm{p,q}}^{-1}\ \mathbf{u}_{\mathrm{q}}^{(\mathrm{N})} \circ \left(\otimes_{k \neq n,\, \mathrm{N}} \mathbf{u}_{\mathrm{q}}^{(\mathrm{n})} \right), \tag{B.11}$$

where the only nonzero singular value is contained in one of the singular vectors. Then the right singular vector $\mathbf{b}_p^{(N-2)}$ is the estimation of $\otimes_{k \neq n, N} \mathbf{u}_q^{(n)}$ up to a scalar indeterminacy. Then reshaping $\mathbf{b}_p^{(N-2)}$ to a matrix $\mathbf{B}_p^{N-3}$ of size $(I_{N-1}, I_{N-2} \times \cdots \times I_{n+1} \times I_{n-1} \times \cdots \times I_1)$, and from the procedure above we have

$$\mathbf{B}_p^{N-3} = \mathbf{y}_p^{(N)} \circ \mathbf{y}_{\mathrm{p}}^{(\mathrm{N}-1)} \circ \mathbf{b}_{\mathrm{p}}^{(\mathrm{N}-3)} = \mathbf{c}_{\mathrm{p,q}}^{-1}\ \mathbf{u}_{\mathrm{q}}^{(\mathrm{N})} \circ \left(\otimes_{k \neq n,\, \mathrm{N,\, N}-1} \mathbf{u}_{\mathrm{q}}^{(\mathrm{n})} \right). \tag{B.12}$$

Then repeating the procedure several times we finally have

$$\mathbf{y}_p^{(N)} \circ \ldots \circ \mathbf{y}_{\mathrm{p}}^{(\mathrm{n}+1)} \circ \mathbf{y}_{\mathrm{q}}^{(\mathrm{n}-1)} \circ \ldots \circ \mathbf{y}_{\mathrm{p}}^{(1)} = \mathbf{c}_{\mathrm{p,q}}^{-1}\ \mathbf{u}_{\mathrm{q}}^{(\mathrm{N})} \circ \ldots \circ \mathbf{u}_{\mathrm{q}}^{(\mathrm{n}+1)} \circ \mathbf{u}_{\mathrm{q}}^{(\mathrm{n}-1)} \circ \ldots \circ \mathbf{u}_{\mathrm{q}}^{(1)} \tag{B.13}$$

Then from (B.6) and (B.13) we have

$$\mathbf{y}_p^{(N)} \circ \mathbf{y}_{\mathrm{p}}^{(\mathrm{N}-1)} \circ \ldots \circ \mathbf{y}_{\mathrm{p}}^{(1)} = \mathbf{u}_{\mathrm{q}}^{(\mathrm{N})} \circ \mathbf{u}_{\mathrm{q}}^{(\mathrm{N}-1)} \circ \ldots \circ \mathbf{u}_{\boldsymbol{q}}^{(1)}, \tag{B.14}$$

and

$$\| \mathbf{y}_p^{(N)} \|_2 \| \mathbf{y}_p^{(N-1)} \|_2 \ldots \| \mathbf{y}_p^{(1)} \|_2 = \| \mathbf{u}_q^{(N)} \|_2 \| \mathbf{u}_q^{(N-1)} \|_2 \ldots \| \mathbf{u}_q^{(1)} \|_2. \tag{B.15}$$

Then, we finally established a one-to-one correspondence between any estimated component and one latent component. The two equations above extended the back-projection to N-way CPD by eliminating the indeterminacies, i.e. the scalar indeterminacy, and calculating the energy of *pth* estimated component. The polarity indeterminacy of any feature from any mode could also be eliminated by projecting the coefficients to it (the N-way extension of Equation (16)):

$$y_{i_2 p}^{(2)} \cdot \ldots \cdot y_{i_N p}^{(3)} \cdot \mathbf{y}_p^{(1)} = u_{i_2 q}^{(2)} \cdot \ldots \cdot u_{i_N q}^{(3)} \cdot \mathbf{u}_q^{(1)}. \tag{B.16}$$